The Astrophysical Journal Letters, 723:L17–L21, 2010 November 1 doi:10.1088/2041-8205/723/1/L17

ENHANCED DETECTABILITY OF PRE-REIONIZATION 21 cm STRUCTURE

Marcelo A. Alvarez[1], Ue-Li Pen[1], and Tzu-Ching Chang[1,2]
[1] Canadian Institute for Theoretical Astrophysics, University of Toronto, 60 St. George St., Toronto, ON M5S 3H8, Canada; malvarez@cita.utoronto.ca
[2] IAA, Academia Sinica, P.O. Box 23-141, Taipei 10617, Taiwan
Received 2010 June 30; accepted 2010 September 20; published 2010 October 7

ABSTRACT

Before the universe was reionized, it was likely that the spin temperature of intergalactic hydrogen was decoupled from the cosmic microwave background (CMB) by UV radiation from the first stars through the Wouthuysen–Field effect. If the intergalactic medium (IGM) had not yet been heated above the CMB temperature by that time, then the gas would appear in absorption relative to the CMB. Large, rare sources of X-rays could inject sufficient heat into the neutral IGM, so that $\delta T_b > 0$ at comoving distances of tens to hundreds of Mpc, resulting in large 21 cm fluctuations with $\delta T_b \simeq 250$ mK on arcminute to degree angular scales, an order of magnitude larger in amplitude than that caused by ionized bubbles during reionization, $\delta T_b \simeq 25$ mK. This signal could therefore be easier to detect and probe higher redshifts than that due to patchy reionization. For the case in which the first objects to heat the IGM are QSOs hosting $10^7\,M_\odot$ black holes with an abundance exceeding $\sim$1 Gpc^{-3} at $z \sim 15$, observations with either the Arecibo Observatory or the Five Hundred Meter Aperture Spherical Telescope could detect and image their fluctuations at greater than 5σ significance in about a month of dedicated survey time. Additionally, existing facilities such as MWA and LOFAR could detect the statistical fluctuations arising from a population of $10^5\,M_\odot$ black holes with an abundance of $\sim 10^4$ Gpc^{-3} at $z \simeq 10$–12.

Key words: cosmology: theory – dark ages, reionization, first stars – intergalactic medium

1. INTRODUCTION

The 21 cm transition is among the most promising probes of the high-redshift universe. The observed differential brightness temperature from the fully neutral intergalactic medium (IGM) at the mean density with spin temperature $T_s(z)$ is given by

$$\delta T_b(z) \simeq 29\,\mathrm{mK}\left(\frac{1+z}{10}\right)^{1/2}\left[1-\frac{T_{\mathrm{CMB}}(z)}{T_s(z)}\right] \quad (1)$$

(e.g., Madau et al. 1997). In the absence of an external radiation field, only hot, dense gas in minihalos would have been able to develop a spin temperature different from the cosmic microwave background (CMB) at $z \sim 20$ (Shapiro et al. 2006). However, radiation emitted by the first stars (e.g., Ciardi & Madau 2003; Barkana & Loeb 2005) and X-ray sources (e.g., Tozzi et al. 2000; Chuzhoy et al. 2006; Chen & Miralda-Escudé 2008) could have coupled T_s to the IGM temperature via the "Wouthuysen–Field effect" (Wouthuysen 1952; Field 1959), at redshifts as high as $z = 20$–30, resulting in $\delta T_b \simeq -250$ mK.

Only a modest amount of heating is necessary to raise the gas temperature above the CMB temperature of $\sim$30–60 K at $z \sim 10$–20. By the time reionization was well underway, it is generally believed that the neutral component of the IGM had already been heated to $T_s \gg T_{\mathrm{CMB}}$, so that $\delta T_b \simeq 25$ mK, an order of magnitude lower than when the IGM was in absorption (e.g., Furlanetto et al. 2006).

Clearly, there should be some transition epoch, during which sources of X-ray radiation heated the IGM, creating "holes" in absorption. Natural candidates for this heating are quasars. Previous work investigating the 21 cm signature of quasars, beginning with Tozzi et al. (2000), have generally treated scenarios in which $T_s \gtrsim T_{\mathrm{CMB}}$, so that the highest possible contrast achievable with respect to the background is on the order of $\sim$30 mK (e.g., Chuzhoy et al. 2006; Zaroubi et al. 2007; Thomas & Zaroubi 2008; Chen & Miralda-Escudé 2008). Here, we explore a new scenario, in which $T_s \ll T_{\mathrm{CMB}}$ in the background IGM, so that the contrast provided by the ionization and heating from the quasar leads to a much larger signal, with $\delta T_b \sim 200$–300 mK.

Unfortunately, little is known about quasars at $z > 6$, with the only constraints coming from the bright end at $z \sim 6$ (e.g., Fan et al. 2002; Willott et al. 2010), with inferred black hole masses $\gtrsim 10^8\,M_\odot$, luminosities $\gtrsim 10^{46}$ erg s^{-1}, and a comoving abundance $\gtrsim$1 Gpc^{-3}. Furthermore, high-redshift supernovae (Oh 2001) and X-ray binaries could have also produced X-rays. Models typically parameterize X-ray production associated with star formation by f_X, normalized so that $f_X = 1$ corresponds to that observed for local starburst galaxies (e.g., Furlanetto 2006; Pritchard & Furlanetto 2007).

Our aim is to explore the enhanced 21 cm signature of early quasars. We therefore assume that the first UV sources pumped the IGM, so that $T_s = T_k$ by $z \simeq 20$, but did not heat it, i.e., $f_X \ll 1$. This is certainly plausible, given that most of the X-ray production in local starburst galaxies, for which $f_X = 1$, comes from binary systems (Furlanetto 2006). It is not obvious that very high redshift star formation would also produce X-ray binaries in such abundance, since the first stars are expected to form mostly in isolation (e.g., Abel et al. 2002), although recent work indicates that some fraction of the first stars may have formed in binary systems (e.g., Turk et al. 2010). The efficiency of X-ray production associated with high-redshift supernovae is similarly uncertain (e.g., Oh 2001). Even if $f_X > 1$, a significant period during which $T_s = T_k$ and $T_k \ll T_{\mathrm{CMB}}$ is still possible (Pritchard & Loeb 2010). Finally, the first galaxies were likely clustered around the quasars and may have actually increased the sizes of the ionized and heated regions (e.g., Alvarez & Abel 2007), although X-ray-emitting galaxies could have also formed outside the regions that would have been heated by the quasars, making the 21 cm features due to early, rare quasars that we predict here less prominent (e.g., Santos et al. 2010).

This paper is organized as follows. In Section 2, we present our forecasted signal and a brief discussion of the black hole abundance at high redshift. In Section 3, we assess the detectability of the predicted signal under various assumptions about the early quasar population. We end in Section 4 with a discussion of possible survey strategies and requirements for detection. All calculations were done assuming a flat universe with $(\Omega_m h^2, \Omega_b h^2, h, n_s, \sigma_8) = (0.133, 0.0225, 0.71, 0.96, 0.8)$, consistent with *WMAP* 7 year data (Komatsu et al. 2010). Distances are comoving.

2. FORECAST

Our predictions will focus on accreting black holes with $M_{\rm BH} \gtrsim 10^5\,M_\odot$. It is possible that a more abundant population lower masses existed at these early times, left behind as remnants of Pop III stars (Heger et al. 2003), acting as "seeds" for the $z \sim 6$ supermassive black hole population (e.g., Li et al. 2007), and powering "miniquasars" (Madau et al. 2004). However, radiative feedback from the progenitors (Johnson & Bromm 2007) and the accretion radiation itself (Alvarez et al. 2009), would have likely substantially limited their early growth and corresponding X-ray emission. An alternative scenario for forming the seeds is gaseous collapse to black holes with masses greater than $\simeq 10^4\,M_\odot$ in the first halos with virial temperature greater than $\simeq 10^4$ K (e.g., Bromm & Loeb 2003; Begelman et al. 2006). Formation of black holes by this mechanism may have been quite a rare occurrence (e.g., Dijkstra et al. 2008). It is this scenario, in which most accreting black holes in the universe were relatively rare and more massive than $\simeq 10^5\,M_\odot$, that is most consistent with the predictions we make here.

Because heating is a time-dependent effect, we parameterize the total energy radiated during accretion by $E_{\rm tot} = Lt_{\rm qso} = \epsilon M_{\rm BH} c^2$, where $\epsilon = 0.1$. In principle, some of the rest mass energy, i.e., the initial seed mass of the black hole, did not contribute to heating the surroundings, but in general the seed mass is expected to be small compared to the mass of the black hole after it undergoes its first episode of radiatively efficient accretion as a quasar, so we neglect it.

2.1. Quasar Spectral Energy Distribution

We assume that the quasar spectral energy distribution is $S_\nu \propto \nu^{-0.5}$ at $\nu < \nu_b$, and $S_\nu \propto \nu^{-1.5}$ at $\nu > \nu_b$, with $h\nu_b = 11.8$ eV (e.g., Bolton & Haehnelt 2007), approximately consistent with the template spectra of Telfer et al. (2002). If the quasar has a total bolometric luminosity L, then the spectral energy distribution is

$$S_\nu = \frac{L}{4\nu_b}\begin{cases}(\nu/\nu_b)^{-0.5}, & \nu < \nu_b,\\ (\nu/\nu_b)^{-1.5}, & \nu > \nu_b.\end{cases} \tag{2}$$

2.2. The 21 cm Profile Around Individual Quasars

The heating by the quasar is obtained by considering the fraction of radiated energy absorbed per atom

$$\Gamma_{\rm H\,I}(r,z) = \frac{(1+z)^2}{4\pi L r^2}\int_{\nu_{\rm H\,I}}^{\infty} d\nu \frac{S_\nu \sigma_\nu}{h\nu}(h\nu - h\nu_{\rm H\,I})\chi_\nu \exp[-\tau_\nu(r)], \tag{3}$$

where χ_ν is the fraction of photoelectron energy, $h\nu - h\nu_{\rm H\,I}$, which goes into heat, with the rest being lost to secondary ionizations and excitations. In the limit in which the mean IGM ionized fraction corresponds to the residual electron fraction from recombination, $\sim 2 \times 10^{-4}$, $0.1 < \chi_\nu < 0.3$ for all $h\nu > 25$ eV (Shull & van Steenberg 1985). In what follows, we will make the approximation that $\chi_\nu = 0.2$ for all ν (since more efficient heating in a more highly ionized medium would only increase the signal, our choice of $\chi_\nu = 0.2$ is a conservative one), and assume that the energy radiated is $Lt_{\rm qso} \equiv \epsilon M_{\rm BH} c^2$, with $t_{\rm qso}$ short compared to the Hubble time. In this case, the relative brightness temperature is given by

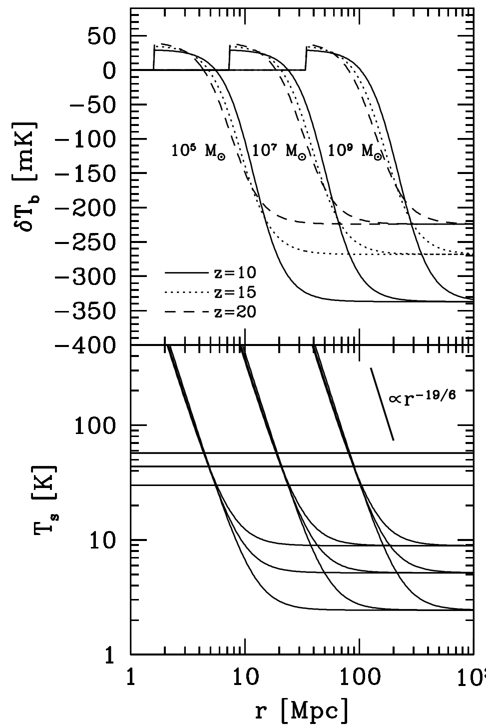

Figure 1. Top: profiles of the observed differential brightness temperature vs. comoving distance at three different redshifts around a quasar that has radiated 10% of the rest-mass energy of 10^5, 10^7, and $10^9\,M_\odot$, as labeled. Note that we have set $\delta T_b = 0$ within the radius of the quasar H II region. Bottom: spin temperature of the IGM, obtained via Equation (5).

$$\delta T_b(M_{\rm BH}, r, z) = 29\,{\rm mK}\left[1 - \frac{T_{\rm CMB}(z)}{T_s(M_{\rm BH}, r, z)}\right]\left[\frac{1+z}{10}\right]^{1/2}, \tag{4}$$

where

$$T_s(M_{\rm BH}, r, z) = T_{\rm IGM}(z) + \frac{2\epsilon M_{\rm BH} c^2}{3k_b}\Gamma_{\rm H\,I}(r,z). \tag{5}$$

We implicitly assume that the IGM is completely neutral at the mean density, $n_{\rm H}(z)$, so that $\tau_\nu(r,z) = r n_{\rm H}(z)(1+z)^{-1}\sigma_\nu$. In reality, the quasar's own H II region, with a radius of $r_{\rm H\,II} \simeq 7.4$ Mpc $(M_{\rm BH}/10^7\,M_\odot)^{1/3}$, determined by equating the total number of ionizing photons released within the lifetime of the quasar with the mean number of hydrogen atoms within the H II region radius, will reduce the opacity at small radii. But given that we are concerned with the small amount of heating happening at much larger radii, we neglect the H II region when calculating the optical depth. This is conservative in the sense that including the reduction in optical depth from the H II region would lead to even more heating at large radius, increasing the spatial extent of the fluctuations we predict.

Profiles of observed differential brightness temperature are shown in Figure 1. The total energy radiated by the quasar, $Lt_{\rm qso}$ in each curve corresponds to 10% of the rest mass, as labeled. Close to the quasar, but outside its H II region the gas is heated to $T_k > T_{\rm CMB}$, and $\delta T_b \simeq$ 30–40 mK. Further away, the heating from the quasar declines due to spherical dilution and attenuation of the lowest energy radiation, with δT_b finally reaching about −220 to −340 mK. The FWHM is about 20, 80, and 400 Mpc for black holes of mass 10^5, 10^7, and 10^9 $M_\odot$, respectively.

2.3. Black Hole Abundance at High z

Willott et al. (2010) constructed the mass function of black holes in the range $10^8\,M_\odot < M_{\rm BH} < 3\times10^9\,M_\odot$ at $z = 6$, finding it to be well fitted by $dn/d\ln M_{\rm BH} \simeq \phi_*(M_{\rm BH}/M_*)^{-1}\exp(-M_{\rm BH}/M_*)$, with $\phi_* = 5.34$ Gpc^{-3} and $M_* = 2.2\times10^9\,M_\odot$. Integrating the black hole mass function, one finds $\rho_{\rm BH}(>M_{\rm BH}) \simeq 7\times10^9$ and $3\times10^{10}\,M_\odot$ Gpc^{-3}, for $M_{\rm BH} = 10^9$, and $10^8\,M_\odot$, respectively, somewhat larger than the black hole mass density we find which maximizes the 21 cm power spectrum (Section 3.2). Matching the abundance of black holes greater than a given mass to the dark matter halo mass function of Warren et al. (2006) at $z = 6$ ("abundance matching"—e.g., Kravtsov et al. 2004), we obtain $M_{\rm halo} = 2.3\times10^{12}$ and $4.7\times10^{12}\,M_\odot$ for $M_{\rm BH} = 10^8$ and $10^9\,M_\odot$, respectively, implying a value of $M_{\rm BH}/M_{\rm halo} \simeq 4\times10^{-5}$ to 2×10^{-4} over the same range.

More detailed predictions require extrapolating the $M_{\rm BH}$–$M_{\rm halo}$ relationship to lower masses and higher redshifts, or making highly uncertain assumptions about the formation mechanism of the high-redshift seeds and their accretion history. For example, the ratio $M_{\rm BH}/M_{\rm halo} \simeq 10^{-4}$ we determine here by abundance matching at $z = 6$ and $M_{\rm BH} = 10^8$–$10^9\,M_\odot$ would be a significant underestimate in atomic cooling halos, where black hole formation by direct collapse took place, in which it is possible that $M_{\rm BH}/M_{\rm halo}$ could approach the limiting value of $\Omega_b/\Omega_m \simeq 0.17$. Clearly, much more work is required in understanding the high-redshift quasar population, and for this reason the constraints provided by either detection or non-detection of the signal we predict here would be very valuable.

3. DETECTABILITY

In this section, we estimate the detectability of individual sources as well the statistical detection of their power spectrum. In the case of individual objects, we focus on a novel approach, using single-dish filled aperture telescopes like Arecibo[3] and Five Hundred Meter Aperture Spherical Telescope (FAST),[4] while for the power spectrum we will simply refer to existing sensitivity estimates for facilities such as LOFAR,[5] MWA,[6] and SKA.[7]

3.1. Individual Quasars

We convolve the profiles shown in Figure 1 with a half-power beam width of

$$\theta_b = 26'\left(\frac{1+z}{11}\right)\left(\frac{d_{\rm dish}}{300\,{\rm m}}\right)^{-1}, \quad (6)$$

where $d_{\rm dish}$ is the effective dish diameter. Converting angle on the sky to comoving distance, we obtain the comoving resolution:

$$D \simeq 70\,{\rm Mpc}\left(\frac{d_{\rm dish}}{300\,{\rm m}}\right)^{-1}\left(\frac{1+z}{11}\right)^{1.2}. \quad (7)$$

3 http://www.naic.edu
4 http://en.bao.ac.cn/node/62
5 http://www.lofar.org
6 http://www.mwatelescope.org
7 http://www.skatelescope.org

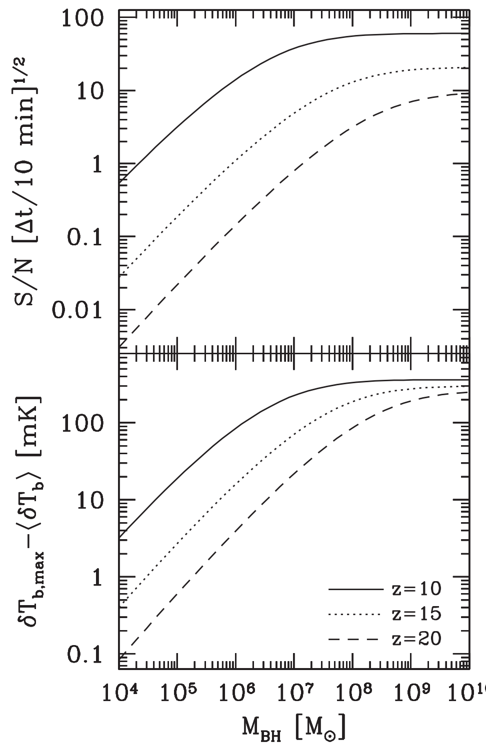

Figure 2. Bottom: peak fluctuation amplitude measured with respect to the mean background absorption $\langle\Delta T_b\rangle(z)$, as a function of black hole mass, for three different redshifts and $d_{\rm dish} = 300$ m. Top: signal-to-noise ratio at the same redshifts for a bandwidth corresponding to the beam width and an integration time of 10 minutes. The detectability declines rapidly in the interval $10 < z < 20$.

This implies that the fluctuation created by a $10^7\,M_\odot$ black hole would be just resolvable with a single 300 m dish like Arecibo (see Figure 1), lower mass black holes would be unresolved, and the profile of higher mass black holes could actually be measured. For an integration time of Δt, the sensitivity is given by

$$\delta T_{\rm err} = 22\,{\rm mK}\left(\frac{\Delta t}{60\,{\rm s}}\right)^{-1/2}\left(\frac{d_{\rm dish}}{300\,{\rm m}}\right)^{1/2}\left(\frac{1+z}{11}\right)^{2.35}, \quad (8)$$

where

$$\Delta\nu = 4\,{\rm MHz}\left(\frac{D}{70\,{\rm Mpc}}\right)\left(\frac{1+z}{11}\right)^{-1/2}. \quad (9)$$

for the bandwidth corresponding to a comoving distance D, $\delta T_{\rm err} = T_{\rm sys}/\sqrt{\Delta\nu\Delta t}$, and $T_{\rm sys} \simeq 3\times10^5$ mK$[(1+z)/11]^{2.7}$ (e.g., Furlanetto et al. 2006).

The maximum fluctuation amplitude, $\delta T_{\rm b,max}(M_{\rm bh}, z)$, is a convolution of the beam with the individual profiles plotted in Figure 1,

$$\delta T_{\rm b,max} = \frac{2}{\theta_g^2 D}\int_0^\infty d\theta\theta e^{-\frac{\theta^2}{2\theta_g^2}}\int_0^{D/2} dl\,\delta T_b(r_{l\theta}), \quad (10)$$

where we use a Gaussian profile with an FWHM of $\theta_b(z)$, such that $\theta_b(z) = 2\sqrt{2\ln 2}\theta_g(z)$, and $r_{l\theta}^2 = r_\theta^2 + l^2$, and r_θ is the projected comoving distance perpendicular to the line of sight corresponding to the angle θ.

Shown in Figure 2 are the resulting fluctuation amplitudes, $\delta T_{\rm b,max}(M_{\rm bh}, z) - \langle\delta T_b\rangle(z)$, as well as the signal-to-noise ratio, $[\delta T_{\rm b,max}(M_{\rm bh}, z) - \langle\delta T_b\rangle(z)]/\delta T_{\rm b,err}(z)$ for an integration time

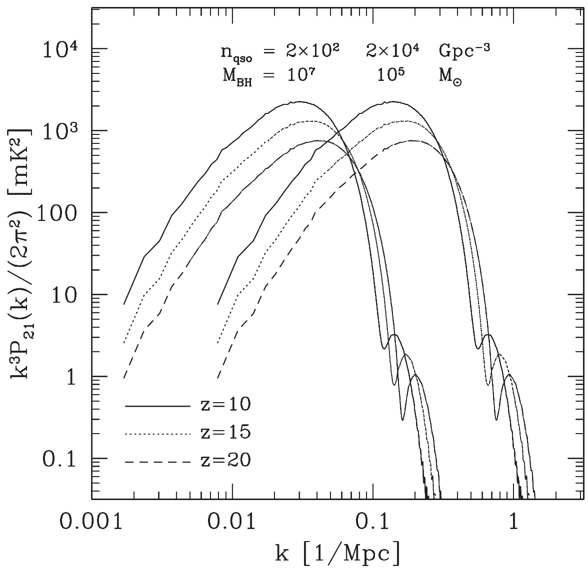

Figure 3. Shown is the spherically averaged three-dimensional power spectrum of 21 cm fluctuations for a black hole density 1 $M_\odot$ Mpc^3, for three different redshifts as labeled. Large, relatively rare $10^7\,M_\odot$ black holes have a power spectrum which peaks at $k \sim 0.03$ Mpc^{-1}, while for $M_{\rm BH} = 10^5\,M_\odot$ the power spectrum peaks at $k \sim 0.15$ Mpc^{-3}. Such a signal at $z = 10$ should be easily detectable by LOFAR, MWA, or SKA.

of 10 minutes. As can be seen from the figure, both the signal and to a greater extent the signal-to-noise decline rapidly with increasing redshift. This is due to several reasons. First, the intrinsic signal declines with increasing redshift because absorption is relatively weaker at higher redshifts when the IGM has not had as much time to cool (see Figure 1). In addition, the beamwidth gets larger in proportion to $1 + z$, while the angular size of the fluctuations at fixed black hole mass actually decline with redshift, as seen from Figure 1.

3.2. Power Spectrum from Poisson Fluctuations

To estimate the fluctuations from a superposition of sources, we assume that all black holes at a given redshift have the same mass, $M_{\rm BH}$, and comoving number density, $n_{\rm BH}$. We then generate a realization of random black hole positions within a periodic box and calculate the heating from each source using Equation (5). Because the heating rate is proportional to mass and we assume a random spatial distribution, the two length scales in the system are the mean separation of sources, $r_{\rm sep} \propto n_{\rm BH}^{-1/3}$, and the distance out to which an individual black hole can effectively heat the IGM above the CMB temperature, $r_{\rm heat} \propto M_{\rm BH}^{1/3}$. For this simplified case, in which the spatial distribution of black holes is random and all black holes have the same mass, the shape of the power spectrum is determined only by the ratio $r_{\rm heat}/r_{\rm sep} \propto (n_{\rm BH} M_{\rm BH})^{1/3} = \rho_{\rm BH}^{1/3}$. Our choice of $\rho_{\rm BH} = 2 \times 10^9\,M_\odot$ Gpc^{-3} is roughly that density at which the signal is maximized; a lower black hole mass density results in a lower overall signal, while a higher density leads to overlap of the individual regions, and the fluctuations become saturated.

Shown in Figure 3 is the power spectrum for Poisson fluctuations, obtained by spherically averaging the Fourier transform of the resulting $\delta T_b(\mathbf{x})$ in k-space. Because the black hole mass density is the same in both cases, the curves have the same shape, but are shifted in wavenumber such that $k^{-3} \propto M_{\rm BH}$. Because individual regions are only weakly overlapping for $\rho_{\rm BH} = 2 \times 10^9\,M_\odot$ Gpc^{-3}, the shape of the curve is quite close to the Fourier transform of an individual region, so that

$$P(k)^{1/2} \propto \int_0^\infty r^2 dr\, \delta T_b(r) \frac{\sin kr}{kr}, \tag{11}$$

with $\delta T_b(r)$ given by Equations (4) and (5).

The amplitude of this signal at $k \sim 0.1$ Mpc^{-1} ($[k^3 P(k)/(2\pi^2)]^{1/2} \simeq 50$ mK) is almost an order of magnitude greater than that expected from ionized bubbles when $T_S \gg T_{\rm CMB}$ ($\simeq 6$ mK, e.g., Furlanetto et al. 2004), which compensates for the increased foregrounds at the higher redshifts corresponding to the signal we predict here. For example, McQuinn et al. (2006) estimated the sensitivity of various facilities to the spherically averaged power spectrum, finding (at $z = 12$) $\delta T^2_{\rm b,err}(k \sim 0.1\ {\rm Mpc}^{-1}) \simeq 30\,{\rm mK}^2$ for LOFAR and MWA, and $T^2_{\rm b,err}(k \sim 0.1\,{\rm Mpc}^{-1}) \simeq 0.1\ {\rm mK}^2$ for SKA, for their adopted array configurations and 1000 hr of integration time (Figure 6 and Table 1 of McQuinn et al. 2006). Thus, the power spectrum shown in Figure 4 would be easily detectable by either of these three experiments at $z \sim 12$ for the survey parameters used by McQuinn et al. (2006).

4. SURVEY STRATEGIES

Since the signal comes from a large angular scale on the sky, a filled aperture maximizes the sensitivity. The two largest collecting area telescopes are Arecibo and, under construction, FAST. They are at latitudes $\delta = 18$ (26) deg, respectively. To stabilize the baselines, a drift scan at 80 MHz maps a strip of width 40 (90) arcmin by length 360 deg $\cos\delta$ every day. With Arecibo, a custom feedline with pairwise correlations of dipoles would allow a frequency-dependent illumination of the mirror, allowing the frequency-independent removal of foregrounds. It would also allow operation as an interferometer, increasing stability and rejection of interference, and enabling arbitrary apodization of the surface. Should grating side lobes from support structures become a problem, one could also remove the carriage house, and mount the feedline on a pole from the center of the dish. This would result in a clean, unblocked aperture with frequency-independent beam. Even with the carriage support blocking, the side lobes would still be frequency independent for an appropriately scaled illumination pattern.

For FAST, a focal plane array also enables a frequency-dependent illumination of the primary, resulting in a frequency-independent beam on the sky. It also increases the survey speed by the number of receivers used. Only one receiver is needed every half wave length, roughly 2 m. Hundred pixel surveys seem conceivable at low cost, since only small bandwidths would be needed, and the system temperature is sky limited, even with cheap TV amplifiers.

We note that the ratio of signal to foreground in this regime is comparable to that during reionization. With a filled aperture, it may be easier to achieve foreground subtraction. This has been demonstrated for intensity mapping at $z \sim 0.8$ using the filled aperture of the Green Bank Telescope (Chang et al. 2010), where a similar foreground ratio exists of galactic synchrotron to 21 cm.

Shown in Figure 4 is the expected number of black holes within the field of view versus their comoving number density. A one month survey at 88 MHz ($z \sim 15$) with a 300 m dish like Arecibo, which scans each point in the sky nine times would have pixel sizes of 0.4 deg^2, implying a pixel integration time of 15 minutes and a survey size of 1140 deg^2. If $10^7\,M_\odot$ black holes had a density of 1 Gpc^{-3}, one would expect to discover about

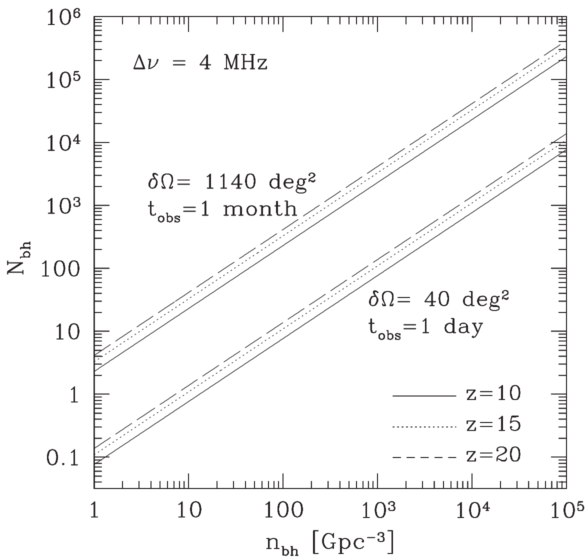

Figure 4. Number of black holes expected within a 1 month (upper curves) and 1 day (lower curves) survey in drift-scan mode that scans each point in the sky nine times, as a function of comoving black hole density. The integration time per pixel in each case is about 7, 14, and 25 minutes for $z = 10$, 15, and 20. With a 14 minute integration time, a $10^7\, M_\odot$ black hole would be detectable at greater than 5σ significance (see Figure 2)

three or four of them at greater than 5σ significance $z = 15$ (see dotted lines in Figures 2 and 4). Such a population could have formed by accretion at the Eddington limit with 10% radiative efficiency from a population of seed black holes with masses $\sim 3 \times 10^5\, M_\odot$ at $z = 30$. This is a plausible scenario, given that the expected abundance of the $10^8\, M_\odot$ atomic cooling halos in which such massive seeds might form is ~ 1 Gpc^{-3} at $z = 30$ (Warren et al. 2006). $M_{BH} > 10^7\, M_\odot$ and similar abundances would be easily detectable, allowing for followup with longer baseline facilities such as LOFAR to determine the detailed shape of their 21 cm profile. Detecting a $10^6\, M_\odot$ black hole at 5σ significance would require a significantly longer integration time on each pixel, about 4 hr, so that only about 70 deg^2 could be surveyed in a month. Thus, the minimum spatial density of $10^6\, M_\odot$ black holes would be about 5 Gpc^{-3} at $z = 15$. Smaller black holes would mean even smaller fields of view and longer integration times per pixel, so in those cases detecting their statistical signature in the spherically averaged power spectrum discussed in Section 3.2 may be a better approach.

We thank J. Peterson and R. M. Thomas for helpful discussions on Arecibo and 21 cm signatures of early QSOs, respectively, and J. R. Pritchard for comments on an earlier draft of the paper. M.A.A. and T.C. are grateful for the hospitality of the Aspen Center for Physics, where this work was completed. We acknowledge financial support by CIfAR and NSERC.

REFERENCES

Abel, T., Bryan, G. L., & Norman, M. L. 2002, Science, 295, 93
Alvarez, M. A., & Abel, T. 2007, MNRAS, 380, L30
Alvarez, M. A., Wise, J. H., & Abel, T. 2009, ApJ, 701, L133
Barkana, R., & Loeb, A. 2005, ApJ, 626, 1
Begelman, M. C., Volonteri, M., & Rees, M. J. 2006, MNRAS, 370, 289
Bolton, J. S., & Haehnelt, M. G. 2007, MNRAS, 374, 493
Bromm, V., & Loeb, A. 2003, ApJ, 596, 34
Chang, T.-C., Pen, U.-L., Bandurak, K., & Peterson, J. B. 2010, Nature, 466, 463
Chen, X., & Miralda-Escudé, J. 2008, ApJ, 684, 18
Chuzhoy, L., Alvarez, M. A., & Shapiro, P. R. 2006, ApJ, 648, L1
Ciardi, B., & Madau, P. 2003, ApJ, 596, 1
Dijkstra, M., Haiman, Z., Mesinger, A., & Wyithe, J. S. B. 2008, MNRAS, 391, 1961
Fan, X., Narayanan, V. K., Strauss, M. A., White, R. L., Becker, R. H., Pentericci, L., & Rix, H.-W. 2002, AJ, 123, 1247
Field, G. B. 1959, ApJ, 129, 536
Furlanetto, S. R. 2006, MNRAS, 371, 867
Furlanetto, S. R., Oh, S. P., & Briggs, F. H. 2006, Phys. Rep., 433, 181
Furlanetto, S. R., Zaldarriaga, M., & Hernquist, L. 2004, ApJ, 613, 1
Heger, A., Fryer, C. L., Woosley, S. E., Langer, N., & Hartmann, D. H. 2003, ApJ, 591, 288
Johnson, J. L., & Bromm, V. 2007, MNRAS, 374, 1557
Komatsu, E., et al. 2010, ApJS, submitted (arXiv:1001.4538)
Kravtsov, A. V., Berlind, A. A., Wechsler, R. H., Klypin, A. A., Gottlöber, S., Allgood, B., & Primack, J. R. 2004, ApJ, 609, 35
Li, Y., et al. 2007, ApJ, 665, 187
Madau, P., Meiksin, A., & Rees, M. J. 1997, ApJ, 475, 429
Madau, P., Rees, M. J., Volonteri, M., Haardt, F., & Oh, S. P. 2004, ApJ, 604, 484
McQuinn, M., Zahn, O., Zaldarriaga, M., Hernquist, L., & Furlanetto, S. R. 2006, ApJ, 653, 815
Oh, S. P. 2001, ApJ, 553, 499
Pritchard, J. R., & Furlanetto, S. R. 2007, MNRAS, 376, 1680
Pritchard, J. R., & Loeb, A. 2010, Phys. Rev. D, 82, 023006
Santos, M. G., Ferramacho, L., Silva, M. B., Amblard, A., & Cooray, A. 2010, MNRAS, 406, 2421
Shapiro, P. R., Ahn, K., Alvarez, M. A., Iliev, I. T., Martel, H., & Ryu, D. 2006, ApJ, 646, 681
Shull, J. M., & van Steenberg, M. E. 1985, ApJ, 298, 268
Telfer, R. C., Zheng, W., Kriss, G. A., & Davidsen, A. F. 2002, ApJ, 565, 773
Thomas, R. M., & Zaroubi, S. 2008, MNRAS, 384, 1080
Tozzi, P., Madau, P., Meiksin, A., & Rees, M. J. 2000, ApJ, 528, 597
Turk, M. J., Abel, T., & O'Shea, B. 2010, Science, 325, 601
Warren, M. S., Abazajian, K., Holz, D. E., & Teodoro, L. 2006, ApJ, 646, 881
Willott, C. J., et al. 2010, AJ, 140, 546
Wouthuysen, S. A. 1952, AJ, 57, 31
Zaroubi, S., Thomas, R. M., Sugiyama, N., & Silk, J. 2007, MNRAS, 375, 1269